JOURNAL OF SPACECRAFT AND ROCKETS
Vol. 43, No. 3, May–June 2006

Efficiency of Electrodynamic Tether Thrusters

J. R. Sanmartin*
Universidad Politécnica de Madrid, 28040 Madrid, Spain
R. D. Estes† and E. C. Lorenzini‡
Harvard–Smithsonian Center for Astrophysics, Cambridge, Massachusetts 02138
and
S. A. Elaskar§
Universidad Nacional de Córdoba, 2000 Córdoba, Argentina

The performance efficiency of electrodynamic bare tethers acting as thrusters in low Earth orbit, as gauged by the ratio of the system mass dedicated to thrust over mission impulse, is analyzed and compared to the performance efficiency of electrical thrusters. Tether systems are much lighter for times beyond six months in space-tug operations, where there is a dedicated solar array, and beyond one month for reboost of the International Space Station, where the solar array is already in place. Bare-tether propulsive efficiency itself, with the tether considered as part of the power plant, is higher for space tugs. Tether optimization shows that thin tapes have greater propulsive efficiency and are less sensitive to plasma density variations in orbit than cylindrical tethers. The efficiency increases with tape length if some segment next to the power supply at the top is insulated to make the tether potential bias vanish at the lower end; multitape tethers must be used to keep the efficiency high at high thrust levels. The efficiency has a maximum for tether-hardware mass equal to the fraction of power-subsystem mass going into ohmic power, though the maximum is very flat. For space tugs, effects of induced-bias changes in orbit might need to be reduced by choosing a moderately large power-subsystem to tether-hardware mass ratio or by tracking the current-voltage characteristic of the solar array.

Nomenclature

A	=	tether cross-sectional area, m^2
$B_\perp$	=	geomagnetic component perpendicular to orbital plane, T
c	=	jet or exhaust velocity in electrical thrusters, m/s
E_m	=	induced ("motional") electric field, V/m
$\tilde{E}_m$	=	normalized induced field
e	=	electron charge, C
F	=	thrust, N
h	=	distance along tether from bottom, m
I	=	tether current, A
$I_{\rm av}$	=	length-averaged tether current, A
$I_{\rm hc}$	=	hollow cathode current, A
$I_{\rm sp}$	=	specific impulse, s
i	=	ratio of current to short-circuit current
L	=	tether length, m
$L_{\rm bt}$	=	length of tether segment left bare at bottom, m
L^*	=	length gauging ohmic vs bare-tether collection impedances, m
M_d	=	mass dedicated to producing thrust, kg
M_t	=	tether mass, kg
m_e	=	electron mass, kg
$\dot{m}_{\rm hc}$	=	mass flow rate at hollow cathode, kg/s
$\dot{m}_p$	=	propellant mass flow rate, kg/s
N_∞	=	ionospheric plasma density, m^{-3}
p	=	perimeter of tether cross section, m
$S(\varphi_B)$	=	auxiliary function defined in Eq. (16b)
$\boldsymbol{U}_{\rm orb}$	=	satellite velocity, m/s
$V_{\rm hc}$	=	hollow cathode bias, V
W_e	=	supply power, W
W_m	=	magnetic thrust power, W
$\tilde{W}$	=	power-supply to tether-hardware mass ratio
α	=	inverse specific power, kg/W
α_t	=	tether hardware mass factor
ΔV	=	electric bias of tether with respect to plasma, V
Δv	=	velocity increment in rocket missions, m/s
η	=	propulsive efficiency of electric thrusters
$\eta_{\rm eff}$	=	overall tether efficiency
ξ	=	normalized distance from tether bottom
ρ	=	tether density, kg/m^{-3}
σ_c	=	tether conductivity, 1/Ωm
τ	=	thrust duration, s
$\tau_{\rm ep}$	=	characteristic time of electric thrusters, s
φ	=	normalized tether bias
$\omega_{\rm hc}$	=	characteristic "gyrofrequency" of hollow cathode in the geomagnetic field, s^{-1}

Subscripts

A, B, C, D	=	points A, B, C, D in the tether

Received 3 March 2005; revision received 1 August 2005; accepted for publication 1 August 2005. Copyright © 2005 by the American Institute of Aeronautics and Astronautics, Inc. All rights reserved. Copies of this paper may be made for personal or internal use, on condition that the copier pay the $10.00 per-copy fee to the Copyright Clearance Center, Inc., 222 Rosewood Drive, Danvers, MA 01923; include the code 0022-4650/06 $10.00 in correspondence with the CCC.

*Professor, Departamento de Fisica, Escuela Técnica Superior de Ingenieros Aeronáuticos, Pza. C. Cisneros 3.
†Research Associate, MS 80, Geoastronomy Division, 60 Garden Street.
‡Staff Scientist, Geoastronomy Division; currently Professor, Department of Mechanical Engineering, University of Padua, Padua, Italy. Senior Member AIAA.
§Professor, Departamento de Aeronáutica, Consejo Nacional de Investigaciones Cientificas y Tecnicas.

Introduction

ELECTRODYNAMIC (ED) tethers, which produce drag without an external power supply, have been proposed as optimal systems for deorbiting spacecraft in low Earth orbit (LEO) at the end of their operational life.[1] On the other hand, if powered by solar panels, as electrical thrusters are, an ED tether could carry current opposite to the direction of the induced or motional electric field to produce thrust. Because its own and related hardware masses make for a large dry mass, a tether proves to be more attractive the longer the duration of the mission for which it is to be used; a peculiar feature of ED tethers in this respect is their presenting two values of "equivalent" exhaust or jet velocity to play the role of the jet velocity $g_0 I_{\rm sp}$ of electrical thrusters. ED tethers are most suitable

for protracted drag compensation, as required by the International Space Station (ISS), and for repeated use to move payloads to higher orbits, as space "tugs" that could freely deboost to meet a new payload. In this work we examine the overall performance of a thrusting ED tether that collects electrons over a bare segment in the orbital-motion-limited (OML) regime and mission durations that make it definitely preferable to electrical thrusters for what concerns the mass requirements. Work in the past has mostly emphasized engineering aspects of thrusting-tether systems.[2–6]

ED Tethers vs Electrical Thrusters

The simplest figure of merit in comparing space thrusters is the ratio of mass M_d dedicated to producing thrust, to mission impulse, which is the product of thrust duration τ and average thrust F. This ratio should be as small as possible, and it is simply the inverse of the jet velocity in the case of chemical propulsion (ignoring feed and storage for simplicity). For electrical thrusters, M_d consists of the propellant mass $\dot{m}_p\tau$ and the mass of the hardware related to the required electrical power W_e:

$$M_d = \dot{m}_p\tau + \alpha W_e \tag{1}$$

There are basically two cases to consider: the case where a dedicated solar-power system is required, as for a space tug, with α typically a few tens of kg/kW; and the case where the solar-power system is already in place, as for the International Space Station, with α less than 10 kg/kW (Refs. 7 and 8).

Using standard relations $\dot{m}_p = F/c$ and $W_e = Fc/2\eta$, one arrives at

$$M_d/F\tau = 1/c + \alpha c/2\eta\tau \equiv (1/c)[1 + \tau_{\rm ep}(c)/\tau] \tag{2}$$

$$\tau_{\rm ep} \equiv \alpha c^2/2\eta$$

$$\approx 1.14 \times \alpha({\rm kg/kw}) \times (c/30\ {\rm km/s})^2 \times (0.65/\eta)\ {\rm weeks} \tag{3}$$

with values of $c \sim 30$ km/s and $\eta \sim 0.65$ being typical of state-of-the-art ion thrusters; corresponding values for Hall thrusters are $c \sim 15$ km/s, $\eta \sim 0.50$ (Ref. 7). In principle, given any jet velocity the ratio $M_d/F\tau$ approaches a minimum $1/c$ for long thrust durations. Duration, however, might need to be restricted for a number of reasons; for a given τ, there is an optimal jet velocity $c_{\rm opt}(\tau)$ given by the equation $\tau_{\rm ep}(c_{\rm opt}) = \tau$ and yielding a minimum in Eq. (2):

$$M_d/F\tau|_{\rm opt} = 2/c_{\rm opt} = \sqrt{2\alpha/\eta\tau} \tag{2'}$$

which decreases with increasing τ.

Conclusions for the standard mission, characterized by requiring a thruster to impart some velocity increment Δv to a payload, are similar to those resulting from Eq. (2). The classical Tsiolkovsky equation for electrical propulsion takes the form[9]

$$\Delta v = c \times \ell_n\left[\frac{1 + (\tau_{\rm ep}/\tau)}{\text{payload mass ratio} + (\tau_{\rm ep}/\tau)}\right] \tag{4}$$

with $\tau_{\rm ep}(c)$ as in Eq. (3). Again, for a given jet velocity Δv approaches a maximum proportional to c for long missions, whereas for given τ there exists an optimal c making Δv maximum at a $\tau_{\rm ep}/\tau$ value lying not far from unity.

Turning now to the case of an ED tether, the dedicated mass is as follows:

$$M_d = \dot{m}_{\rm hc}\tau + \alpha W_e + \alpha_t M_t \tag{5}$$

with tether mass $M_t = \rho AL$ making a substantial contribution to system mass; a factor $\alpha_t = 2$–3 accounts for directly related hardware (end ballast/deployer). Here $\dot{m}_{\rm hc}$ is expellant mass flow rate at a hollow cathode (HC) that emits an electron current $I_{\rm hc}$ at the top of the tether. Actual power from the solar array might depend on the tether-current response, which is affected by plasma density and geomagnetic changes in orbit, but the power W_e in the second term on the right-hand side of Eq. (5) is assumed to be at design conditions until our discussion of off-design performance.

The power associated with the magnetic thrust $F = LI_{\rm av}B_\perp$ is $W_m = FU_{\rm orb} = LI_{\rm av}E_m$, with $E_m = U_{\rm orb}B_\perp$ the vertical component of the induced electric field. In general, the geomagnetic field has a horizontal component parallel to $\boldsymbol{U}_{\rm orb}$, resulting in a force component, here ignored, that pushes the tether off the orbital plane. We then have

$$M_d/F\tau = 1/(\omega_{\rm hc}L \times I_{\rm av}/I_{\rm hc}) + \alpha U_{\rm orb}/\tau\eta_{\rm eff} \approx \alpha U_{\rm orb}/\tau\eta_{\rm eff} \tag{6}$$

Here $\eta_{\rm eff}$ is an effective or overall propulsive efficiency

$$1/\eta_{\rm eff} \equiv W_e/W_m \times (1 + \alpha_t M_t/\alpha W_e) \tag{7}$$

which takes into account the tether as part of the power-plant (with mass independent of mission duration) and which is smaller than the actual propulsive efficiency W_m/W_e. Also, $\omega_{\rm hc} \equiv B_\perp \times I_{\rm hc}/\dot{m}_{\rm hc}$ appears as a gyrofrequency determined by the geomagnetic field and an equivalent charge-to-mass ratio characterizing the hollow cathode.

Note that, in principle, two velocities in Eq. (6) play the role of jet velocity in Eq. (2). Whereas $2U_{\rm orb} \sim 15$ km/s is comparable to c for electrical thrusters, $\omega_{\rm hc}L \times I_{\rm av}/I_{\rm hc}$ can be up to three orders of magnitude greater: with $B_\perp \sim 0.25$ Gauss in LEO at low or moderate orbit inclination, and $L \times I_{\rm hc}/I_{\rm av} \sim 10$ km typically, a ratio $I_{\rm hc}/\dot{m}_{\rm hc} = 100$ A per mg/s (about the charge-to-mass ratio of hydrogen ions) in a state-of-the-art HC yields $\omega_{\rm hc}L \times I_{\rm av}/I_{\rm hc} \sim$ 25,000 km/s. This allowed us to drop the expellant mass term in Eq. (6) for missions not unreasonably long.[6]

Because system mass for a given impulse will be lower the longer the mission is for both a tether thruster and an electrical thruster, we can take τ and F to be separately equal for the two systems in comparing the required system masses. We then obtain, from Eqs. (6) and (2), for given c,

$$\frac{M_d({\rm tether})}{M_d(c, \text{electr. prop.})} = \frac{2\eta U_{\rm orb}/\eta_{\rm eff}c}{1 + \tau/\tau_{\rm ep}(c)} \tag{8}$$

Tether performance relative to that of the electrical thruster is better the longer the mission. A tether system, with $\eta_{\rm eff} \sim \frac{1}{3}$ typically, as is later shown, would be twice as light as a standard ion-thruster system ($c \sim 30$ km/s $\approx 4U_{\rm orb}$) for mission duration $\tau = \tau_{\rm ep}(c)$, or $\tau({\rm weeks}) \sim \alpha$ (kg/kW) from Eq. (3). This is about a half-year for the space tug ($\alpha \sim 25$ kg/kW) and one month for ISS reboost ($\alpha \sim 5$ kg/kW).

For the optimal electrical thruster at given τ, Eqs. (6) and (2′) yield

$$\frac{M_d({\rm tether})}{M_d(c_{\rm opt}, \text{electr. prop.})} = \frac{\eta}{\eta_{\rm eff}}\sqrt{\frac{\tau_{\rm ep}(U_{\rm orb})}{\tau}}$$

$$= \frac{1}{4}\sqrt{\frac{0.74\eta}{\eta_{\rm eff}^2}}\sqrt{\frac{\alpha({\rm kg/kW})}{\tau({\rm weeks})}} \tag{8'}$$

the relative tether performance also improving with mission duration. A tether system would again be twice as light for $\tau({\rm weeks}) \sim \alpha$ (kg/kW), with $c_{\rm opt} \sim 4U_{\rm orb}$ for both space tug and ISS. Note that, in general, for system masses comparable, Eqs. (2′) and (6) give $c_{\rm opt} \approx \sqrt{(\tau/\alpha)} \propto U_{\rm orb}$.

Propulsive Efficiency of ED-Tether Thrusting

Figure 1 shows the configuration of a thruster system using a bare tether. At the top of the tether, there is a power supply to bias the tether positive, against the induced electric field E_m. Electrons flow upward to the top where they are ejected by the hollow cathode, which has a bias voltage $V_{\rm hc}$ with respect to the plasma that typically amounts to at most a few percent of E_mL. We shall set $V_{\rm hc}$ equal to zero in what follows; note that we are also ignoring the small radiation impedance for circuit closure in the ionosphere.

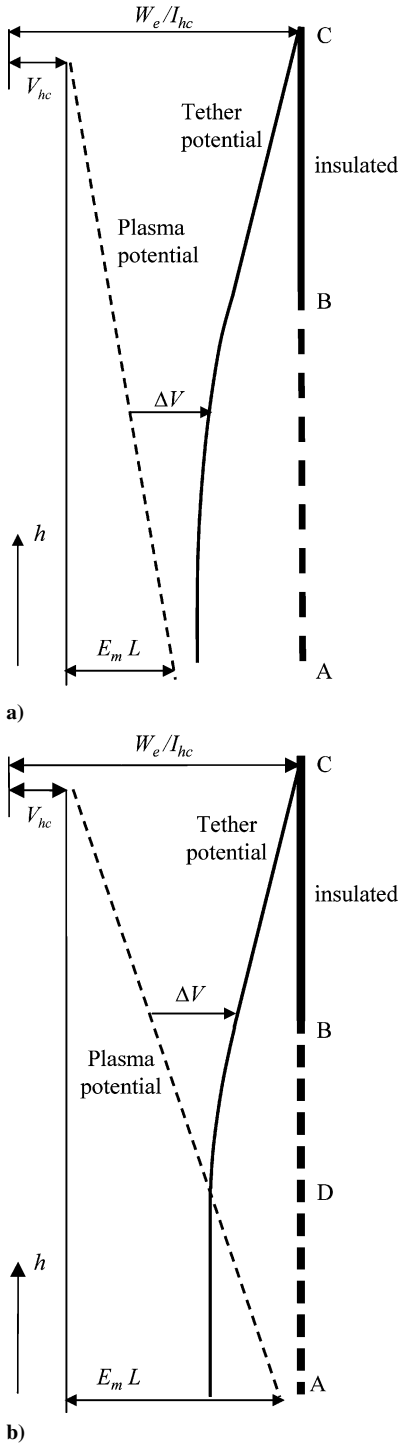

Fig. 1 Tether bias ΔV diagrams; point C is at tether top, A at bottom, and BC is an insulated segment: regimes a) $\Delta V_A > 0$ and b) $\Delta V_A < 0$.

Tether bias ΔV with respect to the local plasma varies along the tether because of both induced and ohmic voltage drops:

$$\frac{\mathrm{d}\Delta V}{\mathrm{d}h} = E_m + \frac{I}{\sigma_c A} \tag{9}$$

Because ΔV increases monotonically from bottom to top in Eq. (9), the average current, which determines the magnetic force, would (in the case where the tether was fully bare) be a small fraction of the current reaching the top, which determines the supply power tapped. This could easily result in a low efficiency η_{eff}. Therefore, only some lower segment AB of length L_{bt} will be left bare.

Bias at the bottom A will vary along the orbit, ΔV_A possibly taking both positive and negative values. In the $\Delta V_A > 0$ regime, electrons are collected over the entire bare segment from A to B, with $I_A = 0$ (Fig. 1a). For $\Delta V_A < 0$, electrons are collected over a segment DB, with D the zero-bias point; because the current vanishes at A, and (ion) collection along the segment AD is very small, we can set $I_D \approx 0$ (Fig. 1b). An analysis of bias and current profiles along the tether is now needed for fully determining η_{eff} (and the ratio $I_{\text{av}}/I_{\text{hc}}$ if desired):

The electrical power is

$$W_e = I_{\text{hc}}\Delta V_C = I_{\text{hc}}[(E_m + I_{\text{hc}}/\sigma_c A) \times (L - L_{\text{bt}}) + \Delta V_B] \tag{10}$$

where we have integrated Eq. (9) from B to C with $I = \text{const} = I_B = I_{\text{hc}}$, so as to relate ΔV_C to ΔV_B. Next, taking the current $I(h)$ from Eq. (9) one finds the magnetic power

$$W_m = E_m I_{\text{av}} L = E_m \int_A^C I\,\mathrm{d}h = I_{\text{hc}} E_m (L - L_{\text{bt}}) + \sigma_c E_m A \times (\Delta V_B - \Delta V_A - E_m L_{\text{bt}}) \tag{11a}$$

for ΔV_A positive. In the ΔV_A negative regime, on the other hand, one finds

$$W_m = I_{\text{hc}} E_m (L - L_{\text{bt}}) + \sigma_c E_m A \times (\Delta V_B - E_m L_{\text{DB}}) \tag{11b}$$

Finally, between A, or D, and B the current is given by the OML law,

$$\frac{\mathrm{d}I}{\mathrm{d}h} = \left(\frac{p}{\pi}\right) e N_\infty \sqrt{\frac{2e\Delta V}{m_e}} \tag{12}$$

We introduce convenient dimensionless variables[10]

$$i \equiv I/(\sigma_c E_m A), \qquad \xi \equiv h/L^*, \qquad \varphi \equiv \Delta V/\left(E_m L^*\right)$$

with a characteristic length L^*, defined by

$$L^*(p/\pi) e N_\infty \sqrt{2eE_m L^*/m_e} = \tfrac{3}{4}\sigma_c E_m A \tag{13}$$

that gauges the bare-tether collection impedance against the tether resistance and depends on the A/p cross-section ratio, ambient conditions, and tether conductivity. Equation (13) expresses that a tether of length L^* at uniform bias $E_m L^*$ would collect a current equal to the short-circuit current, with the factor $\frac{3}{4}$ introduced to simplify the resulting dimensionless equations. The tether collection impedance can be neglected in case of a small ratio L^*/L. For aluminum one has

$$L^* \approx 2.66\ \text{km} \times (E_m/100\ \text{V/km})^{\frac{1}{3}} \times \left[(2A/p \times 0.1\ \text{mm}) \times 10^{11}\ m^{-3}/N_\infty\right]^{\frac{2}{3}} \tag{13'}$$

Equations (9) and (12) now become

$$\frac{\mathrm{d}\varphi}{\mathrm{d}\xi} = 1 + i \tag{14a}$$

$$\frac{\mathrm{d}i}{\mathrm{d}\xi} = \frac{3}{4}\sqrt{\varphi} \tag{14b}$$

with a first integral $\varphi^{3/2} - (2i + i^2) = \text{const}$ (Ref. 10). For $\Delta V_A > 0$, evaluating that first integral at A and B yields

$$\varphi_B^{\frac{3}{2}} - \varphi_A^{\frac{3}{2}} = 2i_{\text{hc}} + i_{\text{hc}}^2 \tag{15a}$$

also, the first integral can be used to integrate the bias equation (14a) from A to B, giving

$$\frac{L_{\text{bt}}}{L^*} = \int_{\varphi_A}^{\varphi_B} \frac{\mathrm{d}\varphi}{\sqrt{1 + \varphi^{\frac{3}{2}} - \varphi_A^{\frac{3}{2}}}} \tag{16a}$$

For $\Delta V_A < 0$, evaluating the first integral at D and B yields

$$\varphi_B^{\frac{3}{2}} = 2i_{\rm hc} + i_{\rm hc}^2 \tag{15b}$$

one also finds

$$\frac{L_{\rm DB}}{L^*} = \int_0^{\varphi_B} \frac{{\rm d}\varphi}{\sqrt{1+\varphi^{\frac{3}{2}}}} \equiv S(\varphi_B) < \frac{L_{\rm bt}}{L^*} \tag{16b}$$

In both regimes the overall propulsive efficiency $\eta_{\rm eff}$ is a function of four dimensionless numbers dependent on environment and tether-system parameters:

$$\tilde{E}_m \equiv E_m\sqrt{\alpha\sigma_c/\alpha_t\rho}, \qquad \tilde{W} \equiv \alpha W_e/\alpha_t M_t$$

$$L_{\rm bt}/L, \qquad L^*/L \qquad \text{or} \qquad L^*\big/L_{\rm bt}$$

whereas the dimensionless average current $i_{\rm av}$ is a function of just three $\tilde{W}/\tilde{E}_m^2$, $L_{\rm bt}/L$, and L^*/L. Note that $\tilde{W}$ is the power-subsystem/tether-subsystem mass ratio and $\tilde{W}/\tilde{E}_m^2$ is the supply-to-ohmic power ratio for short circuit current.

In dimensionless variables Eq. (10) becomes

$$\tilde{W}\big/\tilde{E}_m^2 = i_{\rm hc}\left[(1+i_{\rm hc})(1-L_{\rm bt}/L) + \left(L^*\big/L\right)\varphi_B\right] \tag{17}$$

Next, Eq. (11a) for ΔV_A positive yields

$$i_{\rm av} = (1-L_{\rm bt}/L)i_{\rm hc} + (L^*/L)(\varphi_B - \varphi_A) - L_{\rm bt}/L \tag{18a}$$

Equations (15a), (16a), (17), and (18a) then determine $i_{\rm av}$ vs $\tilde{W}/\tilde{E}_m^2$, $L_{\rm bt}/L$, and L^*/L. As $\tilde{W}$ is decreased with other parameters fixed, a critical value is reached for which φ_A vanishes. For $\tilde{W}$ below that value, that is, for $\Delta V_A < 0$, and using Eq. (16b) in rewriting Eq. (11b) in dimensionless form,

$$i_{\rm av} = (1-L_{\rm bt}/L)i_{\rm hc} + (L^*/L)[\varphi_B - S(\varphi_B)] \tag{18b}$$

Equations (15b), (17), and (18b) again determine $i_{\rm av}(\tilde{W}/\tilde{E}_m^2, L_{\rm bt}/L, L^*/L)$. In either regime, one finds $\eta_{\rm eff}$ by using $i_{\rm av}$ in Eq. (7), which can be rewritten as

$$\eta_{\rm eff} = \frac{\tilde{E}_m^2 i_{\rm av}}{1+\tilde{W}} \tag{19}$$

System Design for Maximum Propulsive Efficiency

For the design conditions in orbit, both $\tilde{W}$ and L^*/L, in addition to the ratio $L_{\rm bt}/L$, can be considered as free parameters. There is, on the other hand, little room for choice in $\tilde{E}_m$, where the ratio $\sqrt{(\alpha_t\rho/\alpha\sigma_c)}$, with $\alpha_t \sim 2.5$ and aluminum as tether material, is about 100 V/km if a dedicated solar-power system is required ($\alpha \sim 25$ kg/kw), and more than twice that if the solar-power system is already in place ($\alpha \sim 5$ kg/kw). Typically, then, $\tilde{E}_m$ will lie in the range of 1–2 in the first case and 0.5–1 in the second case.

Figure 2 shows results for $i_{\rm av}(\tilde{W}/\tilde{E}_m^2)$ at a few values of $L^*/L_{\rm bt}$ and $L_{\rm bt}/L$. Note that the average current $i_{\rm av}$, and even more so the maximum current $i_{\rm hc}$, can exceed unity. Clearly, if it had been driven by the induced field (as in absence of power supply, for deorbit or power generation applications), the maximum current would not exceed the short-circuit value, $I_{\rm hc} < \sigma_c E_m A$ or $i_{\rm hc} < 1$, but sufficiently high power can here produce any value of current. Values for $\tilde{W}$ that are too large, however, lead to low efficiencies.

Figures 3a–3c depict $\eta_{\rm eff}$ vs $\tilde{W}$ for $L_{\rm bt}/L = 1$, 0.6, and 0.3, respectively. Two families of curves are represented in each figure, corresponding to values $\tilde{E}_m = 0.3$, 1, 2.5 and $L^*/L_{\rm bt} = 2$, 1, 0.5, 0.25. The efficiency $\eta_{\rm eff}$ increases monotonically with $\tilde{E}_m$, whereas it exhibits a maximum as a function of $\tilde{W}$. Note, however, that there is still considerable freedom in choosing a design value for $\tilde{W}$ because the maxima in Fig. 3 are very flat. Finally, the efficiency increases as $L_{\rm bt}/L$ decreases and, at the lowest $L_{\rm bt}/L$ ratios, as L^*/L decreases too.

Figure 4 depicts $\eta_{\rm eff}(\tilde{W})$ in the limit $L^*/L = 0$ for a double parametric family $\tilde{E}_m = 0.3$, 1, 2.5 and $L_{\rm bt}/L = 0.3$, 0.1, 0. For each $\tilde{E}_m$ value, $\eta_{\rm eff}$ increases with decreasing $L_{\rm bt}/L$, reaching a maximum in the limit $L_{\rm bt}/L = 0$, independent of the ratio $L^*/L_{\rm bt}$. Now Eqs. (17) and (18a) or (18b) take quite simple forms, with the current uniform along the insulated tether,

$$i_{\rm av} = i_{\rm hc} = i_0\left(\tilde{W}\big/\tilde{E}_m^2\right) \tag{20a}$$

$$i_0(1+i_0) \equiv \tilde{W}\big/\tilde{E}_m^2 \tag{20b}$$

readily yielding $\eta_{\rm eff}(\tilde{W}, \tilde{E}_m)$ in Eq. (19). Maximum efficiency at given $\tilde{E}_m$ is

$$\eta_{\rm eff}({\rm max}) = \tilde{E}_m/(2+\tilde{E}_m) \tag{21a}$$

at

$$\tilde{W} - 1 = 1/i_{\rm av} = \tilde{E}_m \tag{21b}$$

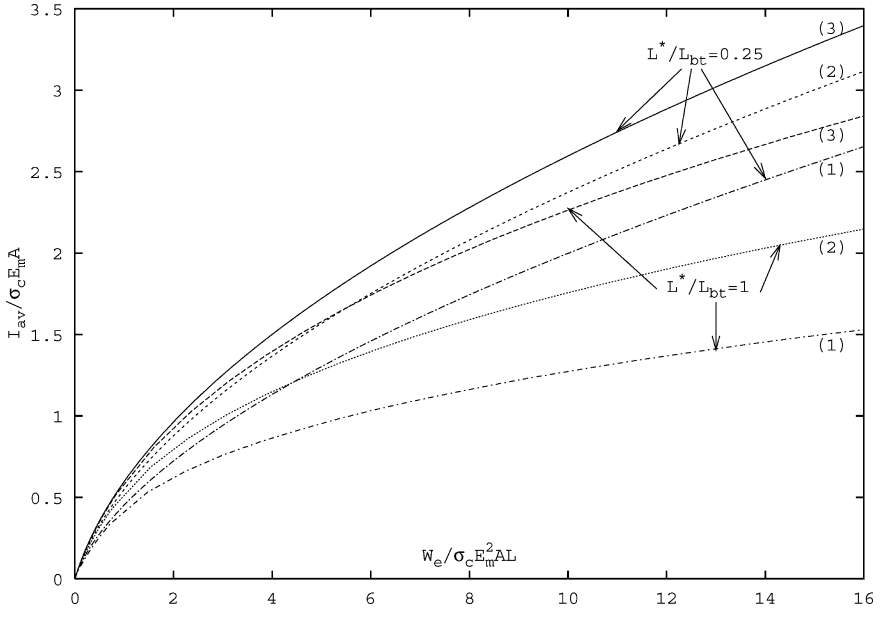

Fig. 2 Length-averaged dimensionless current vs parameter ratio $\tilde{W}/\tilde{E}_m^2$ (supply-to-ohmic power ratio for short-circuit current) for $L^*/L_{\rm bt} = 1$ and 0.25: 1, $L_{\rm bt}/L = 0.6$; 2, $L_{\rm bt}/L = 0.3$; and 3, $L_{\rm bt}/L = 0.1$.

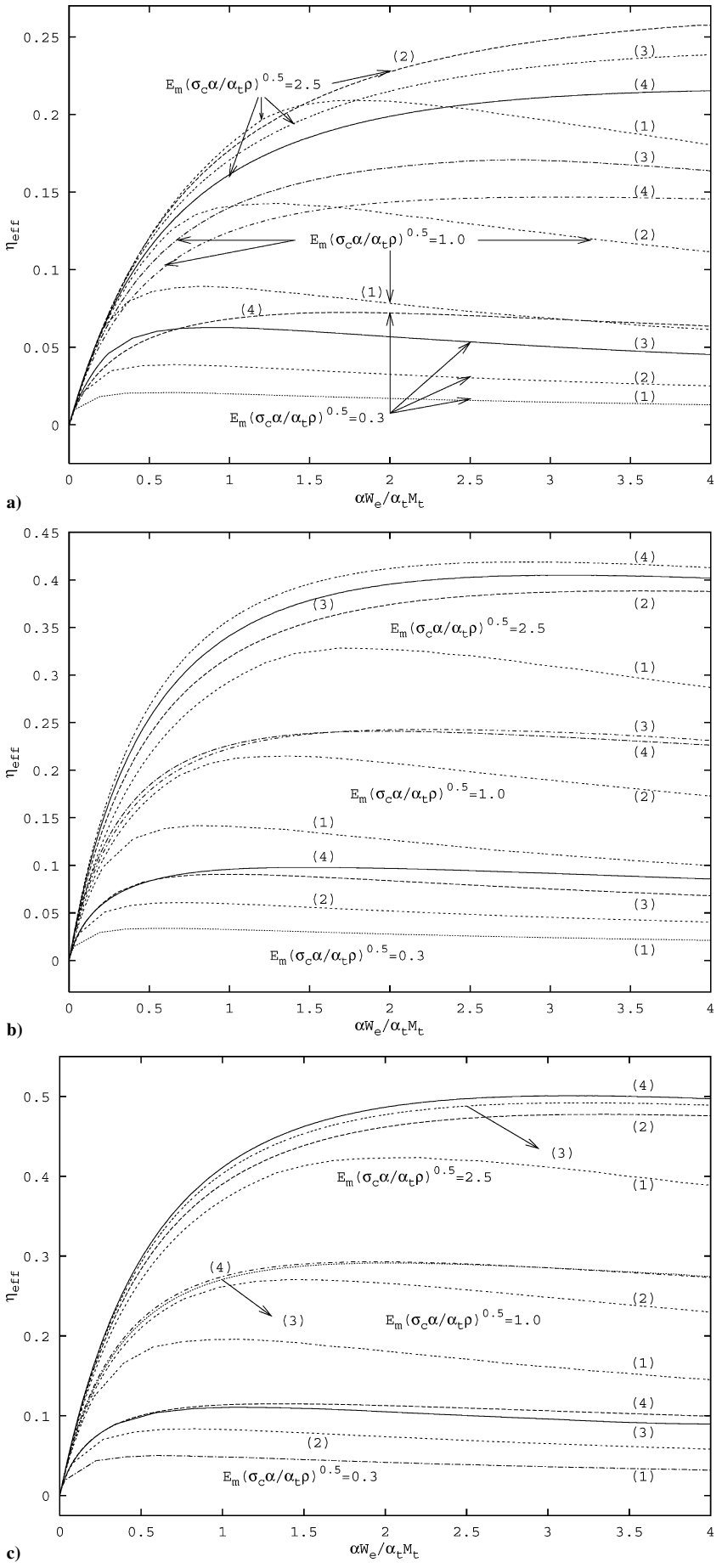

Fig. 3 Overall propulsive efficiency η_{eff} vs parameter $\tilde{W}$ (power-subsystem to tether-subsystem mass ratio) for several values of $\tilde{E}_m$: 1, $L^*/L_{bt} = 2$; 2, $L^*/L_{bt} = 1$; 3, $L^*/L_{bt} = 0.5$; and 4, $L^*/L_{bt} = 0.25$: a) $L_{bt}/L = 1$, b) $L_{bt}/L = 0.6$, and c) $L_{bt}/L = 0.3$.

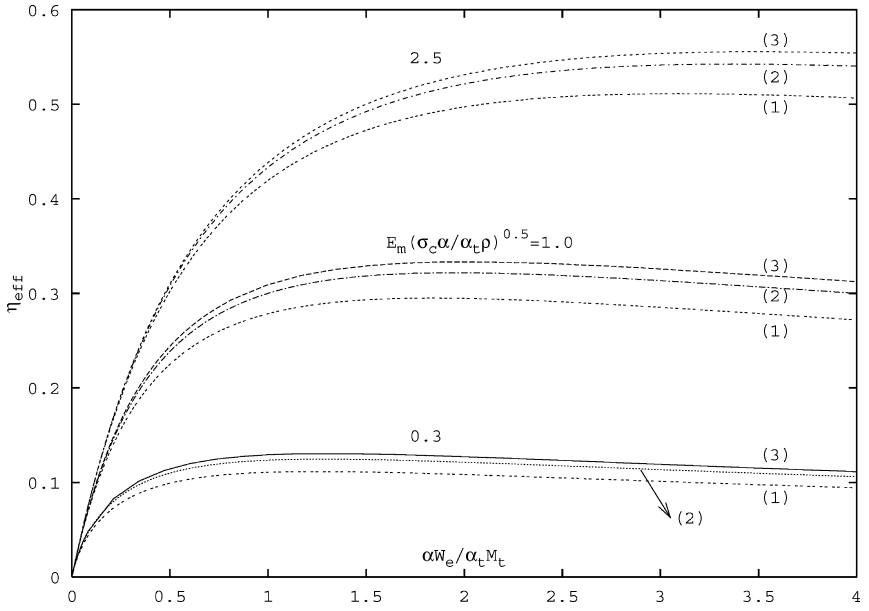

Fig. 4 Overall propulsive efficiency η_{eff} for $L^*/L = 0$ and several values of $\tilde{E}_m$: 1, $L_{\text{bt}}/L = 0.3$; 2, $L_{\text{bt}}/L = 0.1$; and 3, $L_{\text{bt}}/L = 0$.

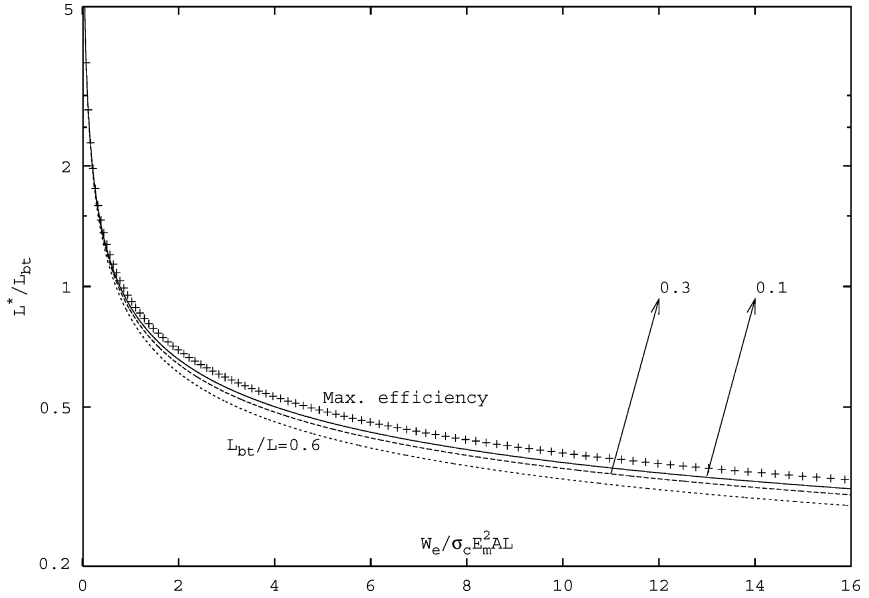

Fig. 5 Ratio L^*/L_{bt} vs $\tilde{W}/\tilde{E}_m^2$ for a few values of L_{bt}/L, such that ΔV_A vanishes. Also shown is the ratio L^*/L_{bt} for maximum efficiency at very small L^*/L and L_{bt}/L.

This is an absolute maximum over the entire $0 < L^*/L, L_{\text{bt}}/L < \infty$ domain. Note that the masses of tether hardware and the ohmic-power fraction in the power subsystem are equal at maximum:

$$\frac{\alpha I_{\text{av}}^2 \times L/\sigma_c A}{\alpha_t M_t} \equiv i_{\text{av}}^2 \tilde{E}_m^2 = 1$$

The ratio L^*/L cannot be made arbitrarily small, however. To determine the optimum ratio L^*/L_{bt} at given small L^*/L, consider first the condition for vanishing bias at the bottom point A. Setting $\varphi_A = 0$ in Eq. (16a), and using Eqs. (15b) and (17), determines a relation $L^*/L_{\text{bt}} = f(\tilde{W}/\tilde{E}_m^2,\ L_{\text{bt}}/L)$. Figure 5 depicts L^*/L_{bt} vs $\tilde{W}/\tilde{E}_m^2$ for a few values of L_{bt}/L. For each value, ΔV_A is positive above and to the right of the corresponding curve, and it is negative below and to the left. Note the very weak dependence of L^*/L_{bt} on the ratio L_{bt}/L.

Setting L_{bt}/L and L^*/L small at fixed $\tilde{W}/\tilde{E}_m^2$, both i_{hc} and i_{av} are given by Eqs. (20a) and (20b) with small corrections linear in L_{bt}/L and L^*/L. Considering the $\Delta V_A \leq 0$ regime in Fig. 5 first, and using Eqs. (15b), (16b), and (18b), one readily arrives at

$$i_{\text{av}} \approx i_0 + \frac{L^*}{L}\left[\varphi_{B0}\frac{1+i_0}{1+2i_0} - S(\varphi_{B0})\right] - \frac{L_{\text{bt}}}{L}\frac{i_0^2}{1+2i_0}$$

with $\varphi_{B0} \equiv \varphi_B(i_0)$ obtained by setting $i_{\text{hc}} = i_0$ in Eq. (15b). Maximum efficiency for given L^*/L clearly requires a minimum L_{bt}/L, which Eq. (16b) shows to occur for $L_{\text{bt}} = L^* \times S(\varphi_B)$, at the corresponding $\Delta V_A = 0$ line in Fig. 5. Then we find

$$i_{\text{av}} \approx i_0 - \frac{L^*}{L} \times \frac{1+i_0}{1+2i_0}[(1+i_0)S(\varphi_{B0}) - \varphi_{B0}] \qquad (22)$$

With the bracketed expression proving to be always positive, Eq. (22) would naturally lead to the previous $L^*/L = 0$, $L_{\text{bt}}/L = 0$ conditions for absolute efficiency maximum.

Actually, one easily verifies that, when moving at constant i_0 (i.e., constant $\tilde{W}/\tilde{E}_m^2$) into the $\Delta V_A > 0$ domain of Fig. 5, where

Eq. (16a) applies, $i_{\rm av}$ first increases with φ_A, then decreases at large φ_A. Maximum efficiency at fixed $\tilde{W}$, $\tilde{E}_m$ occurs at values φ_B and φ_A given by Eq. (15a), with $i_{\rm hc} = i_0$, and

$$\int_{\varphi_A}^{\varphi_B} \frac{\sqrt{\varphi_A}\,{\rm d}\varphi}{\left(1+\varphi^{\frac{3}{2}}-\varphi_A^{\frac{3}{2}}\right)^{\frac{3}{2}}} = \frac{4}{3}\left(\frac{i_0}{1+i_0}\right)^2 \tag{23}$$

using those values in Eq. (16a) determines the optimum ratio $L^*/L_{\rm bt}$, shown in Fig. 5. This ratio is very close to the $\Delta V_A = 0$ curves at small $L_{\rm bt}/L$; its inverse lies in the range of 1–3 except at small $\tilde{W}/\tilde{E}_m^2$, where the L^*/L correction is negligible.

Consider now the changes in power and propulsive efficiency as the tether moves in orbit and operates under off-design conditions. The length $L^* \propto (E_m/N_\infty^2)^{1/3}$ will change mostly through variations in plasma density N_∞ that can be as high as one-and-a-half orders of magnitude, if batteries are charged when in sunlight to allow tethers, like ion thrusters, to work at night. For space tugs, use of batteries may increase the power subsystem mass by more than 50%. A low L^*/L ratio (i.e., high $\eta_{\rm eff}$) makes tether performance less sensitive to N_∞ variations too. Propulsive efficiency $\eta_{\rm eff}$ is weakly dependent on L^*/L and $L_{\rm bt}/L$ if small; also, as orbital conditions move $L^*/L_{\rm bt}$ away from some optimum, making ΔV_A more positive or negative, $\eta_{\rm eff}$ moves away from a maximum, thus dropping weakly. Weak performance changes show the ability of bare tethers to accommodate to electron density variations by self-adjusting the length or just the bias of the segment of tether collecting electrons.[11]

Variations in E_m are more critical for parameter $\tilde{E}_m$ (though the $\tilde{E}_m$ range covered in the figures allows differences in α too, actual E_m variations being less than a factor of two away from some middle design value). In dimensional form, the lowest-order approximation to optimum design, represented by Eqs. (20a) and (20b), can be written as

$$\Delta V_C \approx E_m L + I_{\rm hc}(L/\sigma_c A) \tag{24}$$

showing that both power and efficiency will change with E_m along the orbit unless the power supply tracks a specific point in its current-voltage characteristic $I_{\rm hc}(\Delta V_C)$. Notice that $\tilde{W}$ keeps the design value in Eq. (19) when off design, whereas, in Eq. (17), it involves the changing power actually drawn from the solar array. The E_m effects in Eq. (24) are weak unless $i_{\rm hc}$ is small at design; to accommodate such effects at the highest $\tilde{E}_m$ values would require taking advantage of the flatness of curves $\eta_{\rm eff}(\tilde{W})$ to choose $\tilde{W}$ on the right side of the maximum efficiency.

Consider design values $E_m = 140$ V/km, $N_\infty = 5\times10^{11}$ m^{-3} (midway through typical ranges 100–200 V/km, $10^{11} - 2.5\times10^{12}$ m^{-3}, respectively) and a thin tape of length $L = 20$ km, as in several tethers deployed in orbit in the past, and thickness $\approx 2A/p = 0.1$ mm. We then find from Eq. (13′) $L^* \approx 1.02$ km and $L^*/L \approx 0.05$. Note that the ratio $L^*/L \approx 0.15$ is still small at the lower end of the density range, $N_\infty = 10^{11}$ m^{-3}. Assuming $L_{\rm bt}/L$ also small, Eqs. (20a) and (20b) for the high-efficiency case are approximately valid. Note that a cylindrical tether has a ratio $2A/p =$ radius; if the radius were comparable to tape width, it would be much less efficient than a tape, and if comparable to tape thickness it would provide much less thrust.

Using $\alpha_t = 2.5$, and $\sigma_c \approx 3.5\times10^7/\Omega$m, $\rho \approx 2.7\times10^3$ kg/m^3 for aluminum, and setting $\alpha \sim 5$ kg/kW, we find $\tilde{E}_m \approx 0.71$ for ISS reboost. Equations (21a) and (21b) then yield a maximum efficiency $\eta_{\rm eff} \approx 0.26$, with $i_{\rm av} \approx 1.40$, $\tilde{W} \approx 1.71$, and $\tilde{W}/\tilde{E}_m^2 \approx 3.36$; from Fig. 5 we also find a bare-segment length $L_{\rm bt} \approx 1.82$ km $\ll 20$ km. A tape width of 1 cm would give tether, tether-hardware, and power-subsystem massses $M_t = 54$ kg, $\alpha_t M_t = 135$ kg, and $\alpha W_e = 231$ kg, respectively, for a total mass of 366 kg; current and supply power and voltage would be $I_{\rm av} \approx 6.86$ A and $W_e \approx 46.2$ kW and $\Delta V_c \approx 6.7$ kV. For a geomagnetic field $B \sim 0.2$ Gauss, the Lorentz force, $I_{\rm av} L B \approx 2.74$ N, would be well above the thrust required for continuous ISS reboost. A smaller tether at lower power level would cover reboost.

Next, setting $\alpha \sim 25$ kg/kW we find $\tilde{E}_m \approx 1.59$ for the space-tug case. Equations (21a) and (21b) and Fig. 5 now yield a maximum efficiency $\eta_{\rm eff} \approx 0.44$, with $i_{\rm av} \approx 0.63$, $\tilde{W} \approx 2.59$, $\tilde{W}/\tilde{E}_m^2 \approx 1.02$, and $L_{\rm bt} \approx 1.1$ km. The 1-cm-wide tape would here yield $\alpha W_e = 351$ kg (for a total mass of 486 kg) and $I_{\rm av} \approx 3.09$ A, $W_e \approx 70.2$ kW, $\Delta V_c \approx 22.7$ kV, and $I_{\rm av} L B \approx 1.24$ N. Because $i_{\rm av}$ is now relatively small, it might be convenient to use a higher power to reduce E_m effects; a current $i_{\rm av} \approx 1.4$ would lead to values $\tilde{W}/\tilde{E}_m^2 \approx 3.36$ and $L_{\rm bt} \approx 1.82$ km, $\tilde{W} \approx 8.5$, and $\eta_{\rm eff} \approx 0.37$.

Discussion of Results

The tether/electrical-thruster system-mass ratio for a common mission impulse, as given by Eq. (8) for the case of a fixed jet velocity c, measures their relative performances. For a long enough mission, that ratio decreases as $1/\tau$, the times required increasing as αc^2. Given a state-of-the-art ion thruster with $c \sim 30$ km/s, a tether with overall propulsive efficiency $\eta_{\rm eff} \approx \frac{1}{3}$ is twice as light for half-year space-tug missions (α a few tens of kilograms per kilowatt), and for one-month ISS reboost (α of order of several kilograms per kilowatt). The system-mass ratio takes the simpler form of Eq. (8′) in case of a given mission duration and its optimal jet velocity $c_{\rm opt} \propto \sqrt{(\tau/\alpha)}$. The mass ratio now decreases as $1/\sqrt{\tau}$ for long missions, but it again makes a tether system with $\eta_{\rm eff} = \frac{1}{3}$ twice as light as the electrical thruster, for τ such that $c_{\rm opt}$ is about $4U_{\rm orb} \approx 30$ km/s (half-year for the space tug, one month for ISS reboost).

Our analysis provides a full description of effects of basic design parameters on the propulsive efficiency $\eta_{\rm eff}$. The efficiency exhibits a (very flat) maximum as regards the power-subsystem/tether-hardware mass ratio $\tilde{W}$, reflecting the fact that tether mass and ohmic resistance vary in opposite ways with cross-section area A. The efficiency increases with the dimensionless number $\tilde{E}_m \equiv E_m\sqrt{(\alpha\sigma_c/\alpha_t\rho)}$, which favors aluminum as a material with high conductivity-to-density ratio, and high-α missions. The efficiency $\eta_{\rm eff}$ also increases with a decreasing tether length fraction left bare $L_{\rm bt}/L$ and, at low $L_{\rm bt}/L$, with a decreasing ratio $L^*/L \propto (A/p)^{2/3}/L$, which favors long tethers and a short length L^* characterizing bare-tether collection.

To reduce L^*, one can use a thin tape, the ratio A/p of the tether cross section then being one-half tape thickness. Tapes can be as wide as 12 mm for pure OML-type electron collection.[12] This width is about four times the Debye length in LEO at $N_\infty \approx 10^{12}$ m^{-3} in sunlight conditions, but, actually, the current would be very close to OML values even for densities half an order of magnitude higher.[13] However, moving into greater and greater thrust, with tape width limited by OML-collection considerations and tether current limited by cross-section area, would require thicker tapes; the accompanying A/p increase would then reduce efficiency. This suggests using multitape tethers, each tape with a low A/p ratio, to keep efficiency high when high thrust is required because an analysis of interference between parallel tapes has recently shown it to be low if the tapes are properly spaced.[14]

For any given small L^*/L ratio, there is an optimum value for $L_{\rm bt}/L$ or $L_{\rm bt}/L^*$ yielding maximum efficiency $\eta_{\rm eff}$, which corresponds to a bias at tether bottom ΔV_A that is slightly positive. The optimum ratio $L_{\rm bt}/L^*$ increases with $\tilde{W}/\tilde{E}_m^2$ (supply-to-ohmic power ratio for short-circuit current) and lies typically in the range 1–3; a length $L_{\rm bt}$ too small hinders bare-tether collection, whereas, if too large, it makes ΔV_A highly negative (with point D close to point B in Fig. 1b), thereby making most of the bare-tether segment useless for electron collection. The masses of the tether hardware and the ohmic-power fraction of the power subsystem are equal at the maximum.

In addition to higher efficiency, a low L^*/L ratio makes tether performance less sensitive to N_∞ variations in orbit, showing the ability of bare tethers to accommodate electron density variations. Variations in E_m are more critical at the highest values of the parameter $\tilde{E}_m$; such effects can be reduced by having the power system track a specific point in its current-voltage characteristic, or taking advantage of the flatness of curves $\eta_{\rm eff}(\tilde{W})$ to choose $\tilde{W}$ beyond the efficiency maximum.

Conclusions

ED bare-tether thruster systems are found to be much lighter than electrical thruster systems for times beyond six months in space-tug

operations, where a dedicated solar array is needed, and beyond one month for ISS reboost, where the solar array is already in place. Tether propulsive efficiency itself is higher for a space tug, where tether mass has a smaller effect on performance. Thin tapes, which have low area/perimeter cross-section ratio, exhibit greater propulsive efficiency and are less sensitive to plasma density variations in orbit than cylindrical tethers; a high efficiency requires long, partially insulated tapes, with bias near zero at the bottom. With current limited by cross-section area and width by OML bare-tether collection, a multitape tether, for which analysis has shown little interference between parallel lines, appears to be the best design for keeping efficiency high at high thrust levels. The efficiency has a maximum for tether-hardware mass equal to the fraction of power-subsystem mass going into ohmic power, though the maximum is quite flat. The effects of induced-bias changes in orbit might need to be reduced by choosing a power-subsystem/tether-hardware mass ratio moderately large, or by tracking the current-voltage characteristic of the solar array.

Acknowledgments

Work by J. R. Sanmartin and S. A. Elaskar was supported by the Spanish Ministerios of Ciencia y Tecnologia under Grant BFM01-3723 and Educacion y Cultura under Grant SB01-0080, respectively. The authors acknowledge helpful comments by the reviewers.

References

[1]Ahedo, E., and Sanmartin, J. R., "Analysis of Bare-Tether Systems for Deorbiting Low-Earth-Orbit Satellites," *Journal of Spacecraft and Rockets*, Vol. 39, No. 2, 2002, pp. 198–205.

[2]Estes, R. D., and Lorenzini, E. C., "Performance and Dynamics of an Electrodynamic Tether," AIAA Paper 2000-0440, Jan. 2000.

[3]Pearson, J., Carroll, J., Levin, E., and Oldson, J., "Overview of the ElectroDynamic Delivery Express (EDDE)," AIAA Paper 2003-4790, July 2003.

[4]Hoyt, R. P., Slostad, J. T., and Frank, S. S., "A Modular Momentum-Exchange/Electrodynamic-Reboost Tether System Architecture," AIAA Paper 2003-5214, July 2003.

[5]Sanmartin, J. R., Estes, R. D., and Lorenzini, E. C., "Efficiency of Different Types of ED-Tether Thrusters," *Space Technology and Applications International Forum 2001*, edited by M. S. El-Genk, American Inst. of Physics, New York, 2001, pp. 479–487.

[6]Estes, R. D., Lorenzini, E. C., and Sanmartin, J. R., "Short Tethers for Electrodynamic Thrust," *Space Technology and Applications International Forum 2002*, edited by M. S. El-Genk, American Inst. of Physics, New York, 2002, pp. 548–553.

[7]Martínez-Sánchez, M., and Pollard, J. E., "Spacecraft Electric Propulsion: An Overview," *Journal of Propulsion and Power*, Vol. 14, No. 5, 1998, pp. 688–699.

[8]Estes, R. D., Lorenzini, E. C., Sanmartin, J. R., Pelaez, J., Martinez-Sanchez, M., Johnson, C. L., and Vas, I. E., "Bare Tethers for Electrodynamic Spacecraft Propulsion," *Journal of Spacecraft and Rockets*, Vol. 37, No. 2, 2000, pp. 205–211.

[9]Fortescue, P., and Stark, J., *Spacecraft Systems Engineering*, 2nd ed., Wiley, New York, 1995, Chap. 6.

[10]Sanmartin, J. R., Martinez-Sanchez, M., and Ahedo, E., "Bare Wire Anodes for Electrodynamic Tethers," *Journal of Propulsion and Power*, Vol. 9, No. 3, 1993, pp. 353–360.

[11]Estes, R. D., Sanmartin, J. R., and Martinez-Sanchez, M., "Performance of Bare-Tether Systems Under Varying Magmetic and Plasma Conditions," *Journal of Spacecraft and Rockets*, Vol. 37, No. 2, 2000, pp. 197–204.

[12]Sanmartin, J. R., and Estes, R. D., "The Orbital-Motion-Limited Regime of Cylindrical Langmuir Probes," *Physics of Plasmas*, Vol. 6, No. 1, 1999, pp. 395–405.

[13]Estes, R. D., and Sanmartín, J. R., "Cylindrical Langmuir Probes Beyond the Orbital-Motion-Limited Regime," *Physics of Plasmas*, Vol. 7, No. 7, 2000, pp. 4320–4325.

[14]Sanmartin, J. R., and Estes, R. D., "Interference of Parallel Cylindrical Langmuir Probes," *Physics of Plasmas*, Vol. 8, No. 9, 2001, pp. 4234–4239.

D. Spencer
Associate Editor